Application of EIS to In Situ Characterization of Hydrothermal Sealing of Anodized Aluminum Alloys: Comparison between Hexavalent Chromium-Based Sealing, Hot Water Sealing and Cerium-Based Sealing

A. Carangelo,[a] M. Curioni,[b,*,z] A. Acquesta,[a] T. Monetta,[a] and F. Bellucci[a]

[a] *University of Naples "Federico II", Department of Chemical Engineering, Materials and Industrial Production, 80125 Naples, Italy*
[b] *Corrosion and Protection Centre, School of Materials, The University of Manchester, Manchester M139PL, United Kingdom*

Chromic acid anodizing has been used for almost a century to enhance corrosion protection of aerospace alloys. For some applications, hydrothermal sealing in hexavalent chromium-containing solution is required to enhance further the corrosion resistance but, due to environmental concerns, the use of hexavalent chromium must be discontinued. Good progress has been made to replace chromates during anodizing but comparatively less effort has focused on the sealing process. In this work, for the first time, electrochemical impedance spectroscopy (EIS) has been used to characterize in-situ the sealing processes occurring during hot water sealing, sodium chromate sealing and cerium sealing. The results suggest that the processes occurring during sodium chromate sealing are significantly different compared to hot water and cerium sealing. In particular, during chromate sealing, the porous skeleton is significantly attacked, suggesting that the anticorrosion performance is likely to arise from the residuals of chromate rather than from the improvement of the barrier properties. In contrast, during hot water sealing, little attack occurs on the porous skeleton, and the improved corrosion protection is due to the enhanced barrier effect. During cerium sealing, precipitation of cerium products occurs, providing an inhibitor reservoir, and little, if any, attack occurs on the pre-existing oxide.

Manuscript submitted June 14, 2016; revised manuscript received July 25, 2016. Published August 4, 2016.

Chromic acid anodizing (CAA) is widely used in the aeronautic industry to improve corrosion resistance of aluminum alloys.[1] Since the beginning of the 1990s, however, the high toxicity associated with Cr (VI) has imposed restrictions on their use in industrial applications. As a consequence, numerous attempts have been made to find less toxic alternatives.[2,3]

Anodizing with dilute sulfuric acid (DSA) has been used to obtain thin anodic films (1–5 μm) that provide some protection without excessive deterioration of the fatigue life for specific aerospace alloys. Although the fatigue performance of DSA is acceptable, the corrosion resistance is lower than that of parts anodized in chromic acid (CAA). More recently, a new anodizing procedure, involving the addition of tartaric acid in dilute sulfuric acid electrolyte and called tartaric-sulfuric acid anodizing (TSA), was introduced.[4–6] The addition of tartaric acid to sulfuric acid baths improves significantly the anticorrosive properties of the anodic layers compared to those obtained by sulfuric acid anodizing.[7] Recent work,[7] however, indicates that the mechanism of porous film growth is not significantly affected by tartaric acid additions and that tartaric acid is not incorporated in significant amounts into the oxide material. Thus the corrosion resistance provided by TSA is likely to be associated with residuals of tartaric acid adsorbed on the porous skeleton. Tartaric acid concentration in the order of ppm, has been proved to be effective in reducing both the oxide dissolution rate in acidic environments and the anodic reaction rate. The effect of tartaric acid on the anodic film morphology and corrosion resistance of anodized AA2024-T3 was studied by Boisier et al..[8] Observing the anodized surface by SEM, they suggested that the addition of tartaric acid to the anodizing electrolyte generates anodic films with a reduced porosity. However, this observation might be also due to the reduced chemical dissolution of the external pore regions during anodizing rather than to a difference in the growth mechanism. The latter statement is supported by other works indicating that the presence of tartaric acid in the anodizing electrolyte reduces the growth rate under potentiostatic conditions, but it does not change the anodic film composition, morphology or fundamental growth mechanism.[7,9]

The protective properties of the anodic oxide films formed in TSA is enhanced by addition of rare earth compounds[10,11] having the ability to protect aluminum alloys in several environments. Namely, compounds belonging to the cerium family are environmentally benign and have been proved to be effective when used in protective coatings.[12,13] The main benefits of cerium-based layers are: high corrosion resistance, non-toxicity and a relatively fast deposition process.[14] Gordovskaya et al.[15] showed the formation of cerium-based layers to improve the corrosion resistance of both anodized pure aluminum and AA7075-T6 alloy.

Depending on the applications, anodizing can be followed by hydrothermal sealing. Hydrothermal sealing is a treatment that involves the prolonged immersion of the anodized parts in a suitable electrolyte, generally maintained at elevated temperatures. Such procedure results in the partial hydration of the aluminum oxide that constitutes the porous oxide film.[16] Specifically, during the early stages of hydrothermal sealing, the sealing solution fills the pores, and a layer of hydrated products forms at the pore mouths. This layer separates the solution within the pore from the external solution. Inside the pores, the pore walls partially dissolve, and the internal solution becomes saturated with alumina hydrates. When the temperature is reduced, hydrated alumina precipitates filling the pore and, over time, it crystallizes.[17] The type of electrolyte where sealing is performed has an important impact on the sealing behavior, on the composition and on the protective performance of the resulting layer. For example, simple hot water sealing increases the durability of the anodic film purely due to an improvement of the barrier effect associated with the pore closure. On the other hand, when sealing is performed in hot hexavalent chromium-containing solutions (generally sodium chromate), the re-precipitated products contain significant amounts of hexavalent chromium, and therefore can act as a corrosion inhibitor reservoir.[16,18]

Hexavalent chromium sealing is widely used when corrosion protection is a primary requirement. However, it is an energy intensive process, since the solution must be maintained close to the boiling point, and it has a very significant environmental cost, due to the toxic and cancerogenic nature of the sodium chromate solution.[19] A number of alternatives have been developed in order to reduce the environmental and energy costs associated to sealing, among which the most commons are based on nickel fluoride, nickel acetate or sodium

*Electrochemical Society Member.
[z] E-mail: Michele.Curioni@manchester.ac.uk

Table I. Nominal composition of AA2024-T3 alloy in weight%.

Alloy	Cu	Mg	Mn	Si	Fe	Zn	Ti	Al
2024-T3	4.50	1.44	0.60	0.06	0.13	0.02	0.03	Bal.

acetate. Fluoride ions are used to reduce the temperature of sealing, since they have a strong affinity with aluminum ions and might displace sulfate from the aluminum and promote dissolution.[20] The dissolution of the aluminum oxide generally induces an increase in the pH within the pores. If nickel ions are present, such pH increase can promote the precipitation of nickel hydroxide that fills the pore together with aluminum hydroxide.[20] The various sealing processes, although generally perceived to be broadly similar, i.e. involving the immersion of an anodized part in a hot or warm solution, might be actually significantly different, depending on the operating condition of the sealing bath and on the properties of the oxide to be sealed. Perhaps due to the non-electrochemical nature of the sealing process, little effort has been made, to the authors' knowledge, to develop electrochemical tools that enable following in-situ the evolution of the sealing process. In particular, little information is available on the time evolution of the porous skeleton during sealing in relation to the different sealing electrolytes. Improved understanding of the sealing process and in-situ monitoring capability during sealing would provide an essential tool for the development of environmentally friendly sealing treatments and, importantly, to disclose the relationship between porous oxide characteristics and sealing behavior.

In this work, the sealing behavior in an environmentally-friendly solution containing cerium (III) nitrate and hydrogen peroxide is evaluated in-situ by electrochemical impedance spectroscopy performed during sealing, and compared to the behaviors observed during hot water sealing and sodium chromate sealing.

Experimental

The material used in this study was AA2024-T3 wrought aluminum alloy, with nominal chemical composition given Table I. Specimens were obtained from 1.6 mm thick sheets by guillotine cutting and degreased in acetone. Degreasing was followed by etching in 10 wt% sodium hydroxide at 60°C for 30 s. After etching, the specimens were desmutted in 30 vol.% nitric acid for 15 s at room temperature and dried in a cool air stream. The pretreated specimens were stored in a desiccator until required. Prior to anodizing, the specimens were masked with beeswax, in order to expose an area of 10 cm^2 to the anodizing electrolyte.

Anodizing was undertaken in 0.46 M sulfuric acid with the addition of 80 g/l tartaric acid (TSA). The anodizing electrolyte was gently stirred during the anodizing process. Anodizing was performed at 37°C for 20 min under potentiostatic control following a typical industrial voltage/time cycle (Fig. 1a), which involved an initial voltage ramp, followed by 20 minutes potentiostatic anodizing at 14 V (SCE). A three-electrode cell was used, with the specimen as the working electrode, a saturated calomel reference electrode and an aluminum cathode. After anodizing, the specimens were rinsed repeatedly in deionized water to remove residual acid and dried in a cool air stream. Following anodizing, three different sealing treatments were applied: the first in a solution containing cerium (III) nitrate, the second in a sodium chromate-containing solution and the third in hot water. During sealing, electrochemical impedance spectra were acquired, as described in detail later. As a control for a condition where no sealing occurs, EIS measurements were also performed on as-anodized specimens immersed in cold water with the addition of 1g/l of sodium sulfate, to enhance the electrolyte conductivity during EIS measurement.

The solution for cerium (III) nitrate sealing was prepared with 0.015 M hydrated Ce $(NO_3)_3$, 0.029 M H_2O_2 and deionized water. The hydrogen peroxide was added to increase the deposition rate since it accelerates the oxidation of Ce^{+3} ions to Ce^{+4}, thereby reducing the time required to form the layer and improving its uniformity.[21,15] The specimens were immersed in the solution for 30 min at 37°C.

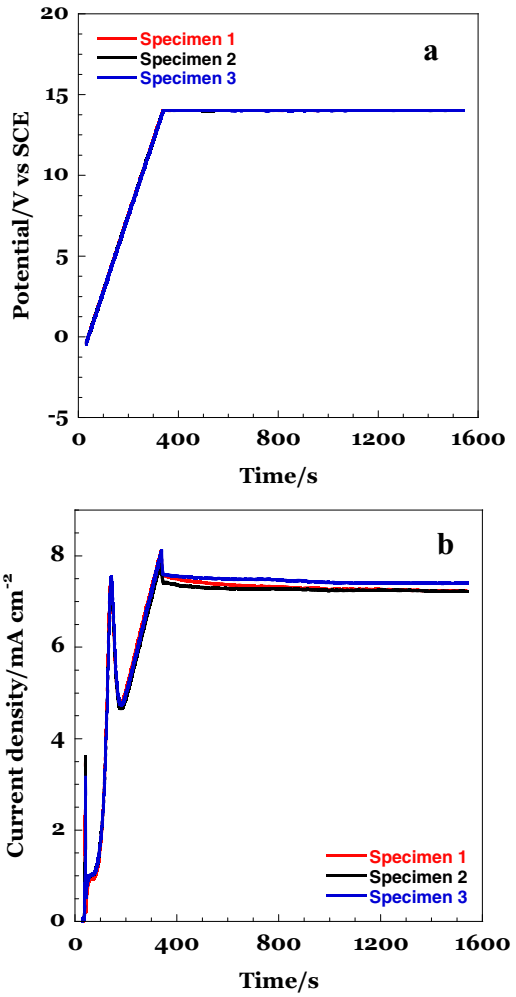

Figure 1. a) Potential and b) current density responses recorded during potentiostatic anodizing of three AA2024-T3 alloys specimens.

Chromate sealing was performed in 70 g/l Na_2CrO_4 and deionized water. The specimens were immersed in this solution for 30 min at 96°C. Hot water sealing was performed in a solution of deionized water, with the addition of 1 g/l of sodium sulfate to increase the conductivity to enable reliable EIS measurements. The pH was corrected at pH = 6 with a few drops of a solution 10 g/l sulfuric acid. The specimens were immersed in this solution for 30 min at 96°C.

The monitoring of the sealing treatment was carried out by EIS. A two-electrode cell was used for the measurement, with one specimen as the working electrode (connected to the working and sense cable of the potentiostat), and another identical specimen as counter electrode and reference electrode (connected to the counter and reference electrode cables of the potentiostat). This two electrode configuration was selected since it enables measurement of the EIS spectra without imposing a constraint on the absolute value of the electrodes potential, as discussed in detail previously.[22] Thus, the perturbation of the sealing process due to the measurement of EIS is minimized, even in conditions where a significant transient in potential occurs.

By using this configuration, the measured impedance is the sum of the impedances of the individual electrodes, since they are placed in series. Under the assumption that the two electrodes are identical (i.e. have identical impedance), the impedance of each electrode (including half of the total solution resistance) can be calculated by dividing by two the measured impedance. The result can be then be normalized

by multiplying by the area of one electrode. Considering that the two electrodes are in series, if the assumption of identical electrodes is violated, for example due to a localized reaction occurring only on one of the two electrodes, the overall response is dominated by the high impedance electrode. This might be an issue during a corrosion measurement, when localization is likely to take place, but it is unlikely to occur during the processes investigated here.

The impedance spectra were acquired continuously, and each acquisition required approximately 6 minutes. Thus, each spectrum represents a 6 minute window in the sealing process, i.e. 0-6 min; 6–12 min; 12–18 min; 18–24 min; 24–30 min. It should be noted that the majority of the time required to acquire an EIS spectrum is needed to obtain the last low-frequency points; thus, the high/medium frequency of the spectrum effectively provides information at 0, 6, 12 minutes and so on. In order to be reliable, EIS measurements require the measured system to be stationary, i.e. that it does not evolve with time. Clearly, the measurement of EIS spectra during sealing is not conducted under stationary conditions, due to the progressive modification of the electrodes surface. If the surface evolves relatively rapidly, as for the systems studied in this work, the reliability of the complete impedance spectra might be questionable. However, considering one by one the points of an impedance spectrum, it is evident that the time required to acquire a point at high frequency is substantially lower than that required to acquire a point at low frequency. Thus, the vast majority of the measurement time is employed for the last few low-frequency points. As a consequence, the high frequency region of the spectrum is intrinsically reliable (since the timescale of evolution of the system is large with respect to the measurement time) whereas the low frequency region is less reliable and might contain artefacts (since the changes on the surface occur on a timescale that is comparable to that of the measurement). In this situation, one can either avoid the acquisition of the spectra, or acquire the spectra even on the non stationary system and then consider critically the results obtained, i.e. remembering that the high frequency regions are intrinsically more reliable than the low-frequency regions.

The specimens were immersed in the respective sealing solutions and the area exposed was 10 cm^2. EIS was performed in potentiostatic mode, applying a sinusoidal potential perturbation with amplitude of 10 mV in the frequency range from 100 kHz to 20 mHz. The DC level between the two identical electrodes was set to 0 V, which is equivalent to short circuiting the two electrodes. After sealing, the specimens were rinsed in deionized water and dried in a cool air stream. Following sealing, EIS was also carried out in cold 1 M Na_2SO_4 solution at room temperature, to characterize the sealed oxides after all the dissolution and precipitation processes had terminated. In this case, a three-electrode cell was used, with the specimen as the working electrode, a saturated calomel reference electrode and an aluminum cathode. The area exposed for these measurements was 2 cm^2. The impedance spectra were acquired in potentiostatic mode at the open circuit potential by applying voltage sinusoidal perturbation with amplitude of 10 mV over the frequency range from 100 kHz to 5 mHz. Before EIS, the open circuit potential was monitored for 15 minute. Each electrochemical test was repeated three times in order to evaluate the reproducibility; generally, very minor differences (of the order of 10% of the impedance modulus), if any, between repeated tests were found.

Scanning Electron Microscopy (SEM) was undertaken by using an EVO 60 microscope operating at an accelerating voltage 20 kV in high vacuum, in order to analyze the surface morphologies of specimens after anodizing and after sealing. The specimens were not metallized prior to observation.

Results

Anodizing response.—The typical anodizing response for the selected anodizing cycle (TSA) is presented in Figure 1b. The current response displayed two peaks during the initial voltage ramp, associated with the oxidation of Al-Mg-Cu and Al-Cu-Fe containing second phase particles, respectively.[23–25] During the initial voltage ramp, the current density increased to about 8 mA/cm^2. As the voltage ramp was interrupted and the constant potential applied, the current decreased slightly, to attain a steady value in the region of 7 mA/cm^2. In Figure 1, three experiments performed in nominally identical conditions are reported, to highlight the good reproducibility of the response.

EIS measurement during sealing.—Results obtained by measuring EIS spectra during the sealing process are reported in Figure 2. Figure 2a displays the results obtained for the control condition, i.e. diluted sulfate solution at room temperature. The spectra display a single time constant, and little, if any, change was observed during the 30 minutes measurement at room temperature. A very similar outcome was revealed when performing the same measurement in hot water (Fig. 2b), with the difference that a resistive behavior in the low-frequency region of the spectra become evident, and a very slight increase in the impedance modulus values with sealing time were observed. During sealing in the chromate-containing solution (Fig. 2c), the behavior was substantially different compared with the two previous cases. Specifically, a significant increase in capacitance (evident as a translation toward the left in the EIS spectra) was revealed between the first measurement, performed immediately after immersion in the hot chromate containing solution, and the second measurement, performed after 6 minutes of immersion. Further, compared to the previous cases, the values of the low-frequency impedance modulus were about two orders of magnitude lower. After 6 minutes, the capacitance values did not change substantially with time, as evident from the spectra overlapping in the medium frequency range, but the low-frequency values of the impedance modulus progressively increased. Sealing in the cerium-containing solution (Fig. 2d) did not result in significant changes in the capacitive response, but produced an increase in the low frequency values of the impedance modulus, that was more significant compared to that observed for hot water sealing.

Comparison of electrochemical impedance spectroscopy response during and post-sealing.—In order to evaluate the phenomena occurring after the sealing is completed, EIS spectra were acquired for all specimens in 1 M sodium sulfate solution at room temperature, shortly after the sealing was completed. In Figures 3a–3c, the EIS spectra acquired on the '*as anodized*' specimens (red, diamonds), during the last 6 minutes of sealing (blue, downward triangles) and after sealing (green, upward triangles) are presented for hot water (a), sodium chromate (b) and cerium (c) sealing treatments.

For hot water sealing (Fig. 3a), it is evident that a second time constant appeared in the medium frequency region of the spectra, associated to the precipitation and solidification of the sealing products. Such time constant only appeared after cooling, and was not evident when the measurement was performed in hot conditions. The capacitive behavior in the medium-low frequency region did not appear to be substantially affected by the sealing. However, the low-frequency part of the spectrum displayed a substantial increase in the values of impedance modulus when the measurement was performed at room temperature. Similar measurements performed during and after chromate sealing displayed a distinctively different behavior (Fig. 3c). Compared to the "*as anodized*" condition, the last measurement in hot chromate solution indicated a substantial increase in capacitance and a substantial decrease in the values of the low-frequency impedance modulus. When the EIS measurement was repeated after sealing in the cold sulfate solution, a slight decrease of the capacitance was evident, accompanied by a substantial increase in the low-frequency values of the impedance modulus, to values comparable to the '*as anodized*' condition. The behavior observed for cerium sealing (Fig. 3c) was somewhat similar to that observed for hot water sealing, i.e. a second time constant appeared after sealing, the capacitive behavior in the medium-low frequency region of the spectra did not change substantially during or after sealing compared to the as anodized condition, and an increase in the low-frequency values of the impedance modulus was observed after sealing. The latter was similar to what was observed for hot water sealing, but the second time constant

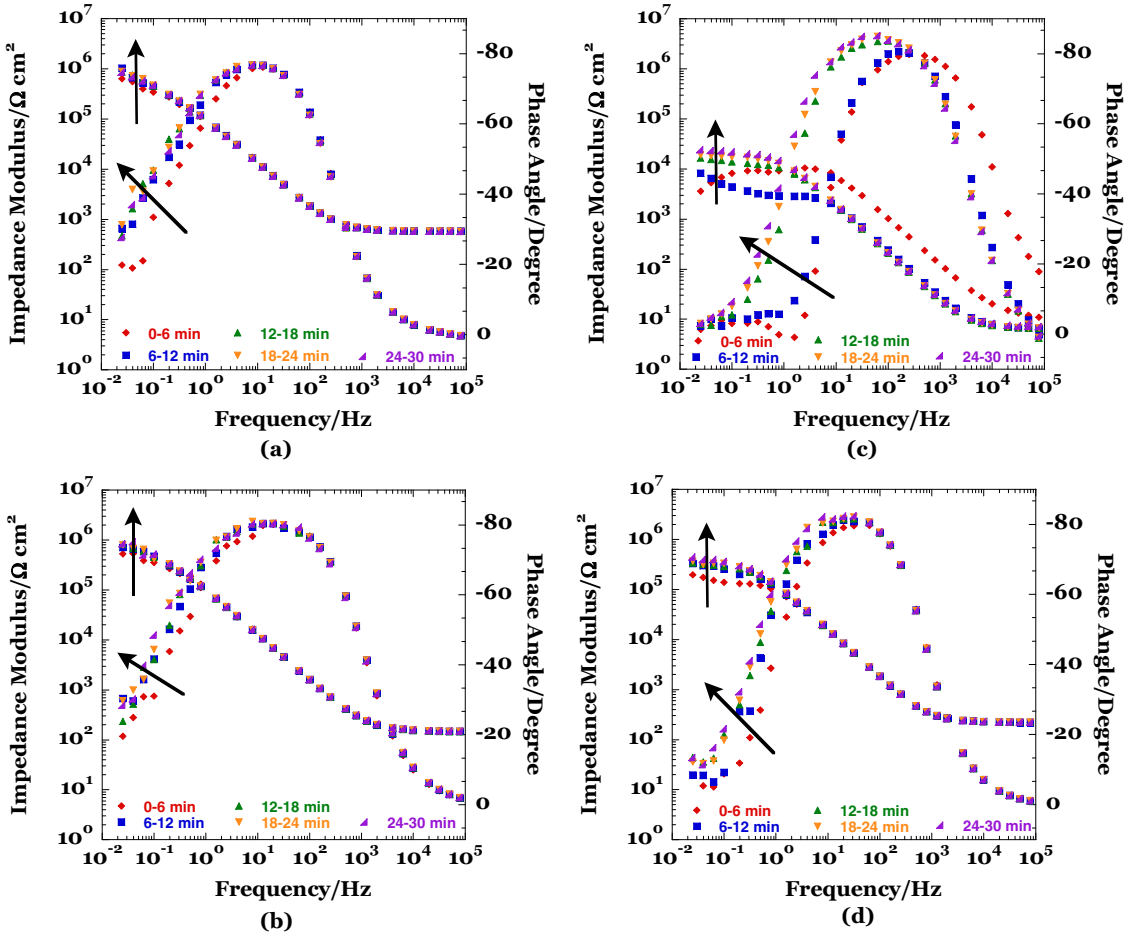

Figure 2. Evolution of impedance modulus and phase angle measured a) in the control condition (cold water), b) during hot water sealing, c) during sodium chromate sealing and d) during cerium (III) nitrate sealing.

was somewhat less evident for cerium sealing compared to hot water sealing.

The overall comparison of the behaviors measured after the various sealing treatments is presented in Figure 4. It is evident that hot water sealing and cerium sealing had little effect on the capacitive behavior at the medium-low frequency range, but both produced a second time constant in the high frequency range. Also, both sealing treatments increased the low-frequency values of the impedance modulus compared to the unsealed conditions. On the other hand, the response of the specimens treated with chromate sealing revealed a significant decrease in capacitance, and values of the low-frequency impedance modulus comparable to those measured without sealing.

Equivalent circuit analysis.—In order to obtain quantitative information from the impedance spectra, two equivalent circuits models were used to fit the data (Fig. 5). Since Hoar and Wood,[26] various equivalent circuits have been proposed to model the EIS response of porous anodic films, particularly the equivalent circuit proposed by Hitzing et al.,[27] which is presented in Figure 5a. In this model, R_s represents the solution resistance, R_w and CPE_w represent resistance and capacitance associated to the pore walls, R_{bl} and CPE_{bl} represent the capacitance and resistance due to the presence of the barrier layer, and R_{seal} and CPE_{seal} represent the capacitance and resistance associated to the presence of sealing products within the pores. Generally, since the thickness of the porous layer is of the order of microns, CPE_w is very low and R_w is very high, therefore the time constant associated with the pore walls is not normally apparent in EIS spectra acquired within the usual frequency ranges. For unsealed porous oxides, the circuit of Figure 5b can be used, and it was employed here to analyze the data obtained during sealing,[8] when the resistance of the sealing products is comparatively low. Constant phase elements were used for the fitting and, values of capacitance for the plots were obtained by using the approach described in Hirschorn, et al.,[28] applicable to a distribution of time constants perpendicular to the electrode surface.

During sealing, the re-precipitated hydroxide layer is likely to contain significant amount of water and is likely to be in the form of gel until it is maintained at high temperature. As a result, the conductivity is relatively high, and the layer cannot be resolved directly by EIS measurement. On the contrary, after cooling, the sealing product precipitate and might crystallize. As a result, ionic migration becomes significantly more difficult compared to the gel products. Thus, the sealing product layer appears as a second time constant in the spectra, and for this reason a circuit that include the resistance and the capacitance associated to the precipitated sealing products (R_{seal} and CPE_{seal}) is used for the fitting, and the circuit of Figure 5c is used to analyze the data. In order to account for the non-planarity of the various layers, constant phase elements are used for the fitting in lieu of ideal capacitors. Figures 6 and 7 show typical calculated (lines) and experimental (symbols) spectra obtained during (Fig. 6) and after (Fig. 7) sealing. The results of the fitting procedure are reported in Tables IIa, IIb.

The time evolution of the barrier layer resistance and of the barrier layer capacitance during sealing, together with the final values obtained after sealing, are presented in Figures 8 and 9, respectively. It is interesting to notice that the both the values of capacitance and resistance measured immediately after immersion for the specimens in cold and hot water were very similar. This indicates that the increase in temperature, per se, does not have a direct effect on the values

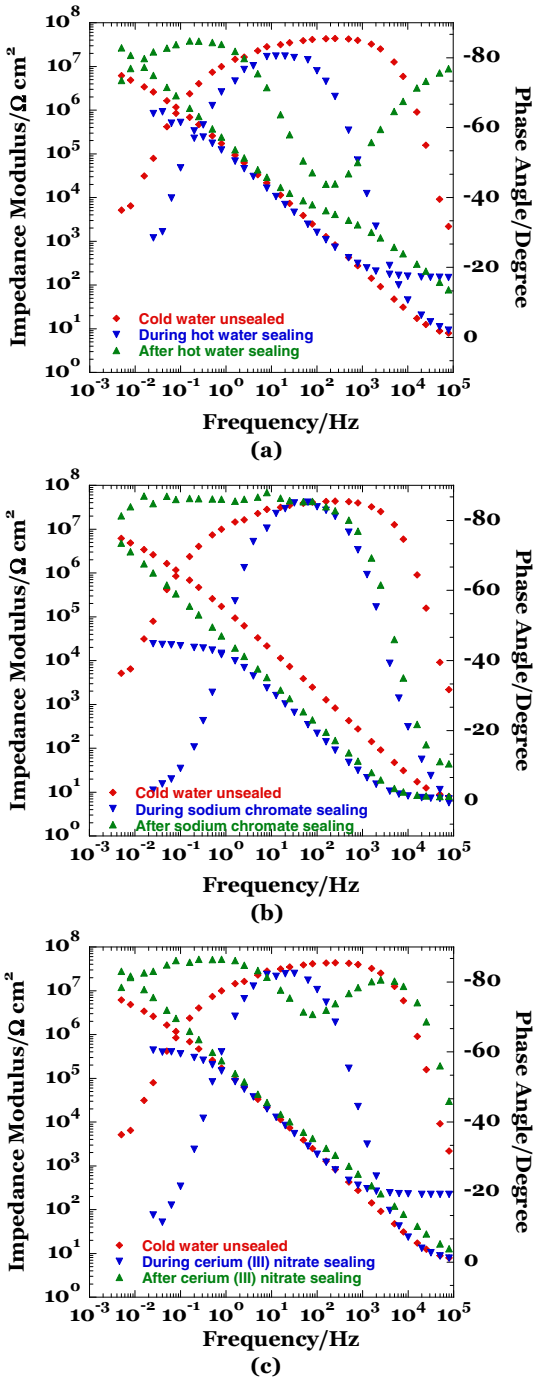

Figure 3. Impedance modulus and phase angle measured during and after a) hot water, b) sodium chromate and c) cerium (III) nitrate sealing.

of capacitance and resistance estimated, since oxide generated under nominally identical conditions (having the same geometry), produce very similar response in terms of resistance and capacitance at both temperatures. For all the sealing treatments, the resistance associated to the barrier layer slightly increased with time during sealing. However, the resistance estimated for the chromate sealing treatment was approximately two orders of magnitude lower than that for all the other conditions. After sealing, the values of resistances for all the three treatments increased substantially, to values of the order of 10^8 ohm $\cdot$ cm^2. The slight increase in the resistance associated with the barrier layer for the unsealed specimens might be attributed to the fact that the process of immersion in the first test electrolyte, followed by

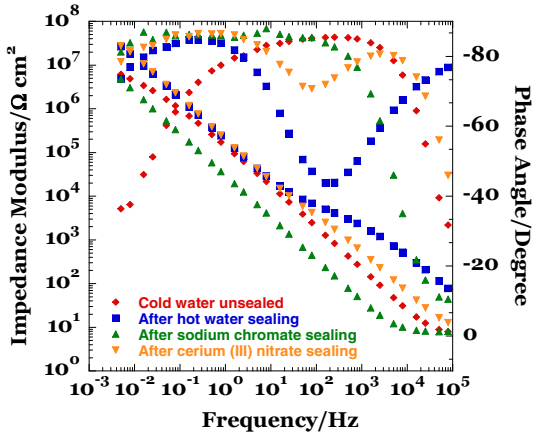

Figure 4. Impedance modulus and phase angle measured after all sealing.

rinsing and drying, might have induced some hydration of the oxide, with subsequent re-precipitation (self-sealing). Such re-precipitation, although not substantial, might have contributed to cover some defects statistically present in the oxide layer. The time evolution of the estimated capacitance associated to the barrier layer is presented in Figure 9. The capacitance inversely correlates with the thickness of the barrier layer beneath the pores. For the control condition, the capacitance was unchanged for all the measurements, as expected since no significant reduction of the barrier layer thickness should occur at low temperatures. The behavior was similar for both hot-water sealing and cerium sealing, although for cerium sealing slightly lower values of capacitance were estimated. After sealing, the capacitances of hot water and cerium-sealed films coincided. Substantially different behavior was observed during chromium sealing. Initially the value of capacitance was similar to that measured for the other treatments but, after 6 minutes, the capacitance increased substantially and remained approximately constant until 30 minutes. After sealing, the capacitance slightly decreased, but it was still higher compared to that measured for the control specimen.

Scanning electron microscopy.—Scanning electron micrographs of specimens after anodizing and after sealing are presented in Figure 10. After anodizing (Fig. 10a), the surface of the anodic oxide reflected the scalloped morphology generated on the alloy by the initial alkaline etching treatment. Cavities and regions of altered film morphology are evident on the surface and associated to the different oxidation behavior of the various metallurgical phases present on the alloy.[23,29,30] After sealing in hot water (Fig. 10b), the surface morphology did not appear substantially different from the one observed on the as-anodized specimen. Conversely, after sealing in chromate-containing solution, the surface of the oxide film appeared substantially modified, with a homogeneous deposit of sealing products clearly evident above the anodic oxide layer. The cerium treatment (Fig. 10d), induced the precipitation of finely dispersed cerium-rich clusters above the porous anodic oxide film. Such cerium-rich deposits on anodized aluminum and aluminum alloy surfaces have been observed previously and characterized in detail by Gordovskaya et al.[15]

Discussion

The sealing process is widely used in the industry to enhance the corrosion protection provided by porous anodic oxides, and it is generally recognized that chromate sealing provides the best anti-corrosion performance, although it has been recently suggested that cerium-based sealing provides good long-term protection. It is generally recognized that the sealing treatments all involve some dissolution of anodic oxide and re-precipitation of sealing process but this work highlights that there are substantial differences between chromium

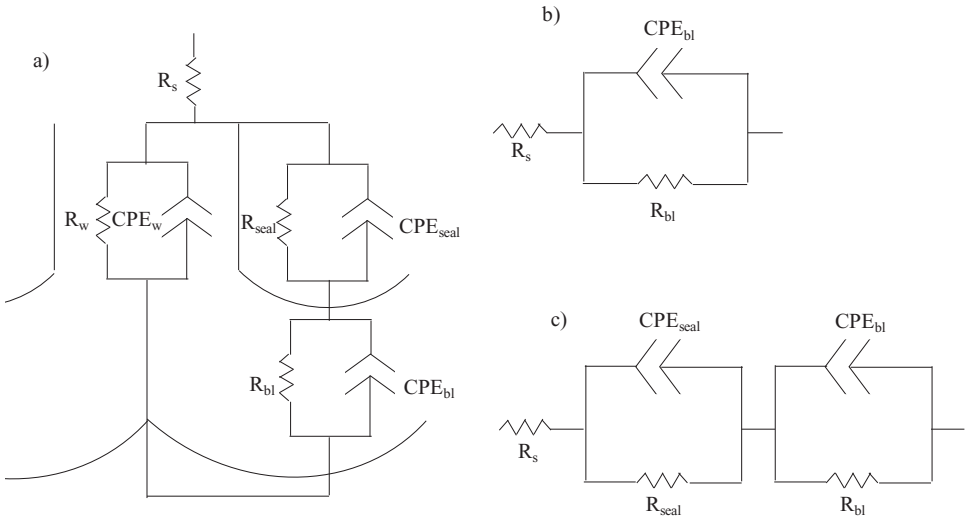

Figure 5. Equivalent circuits representing sealed porous anodic oxide (a) general model, (b) model used to fit the data acquired during sealing and (c) model used to fit the data acquired after sealing.

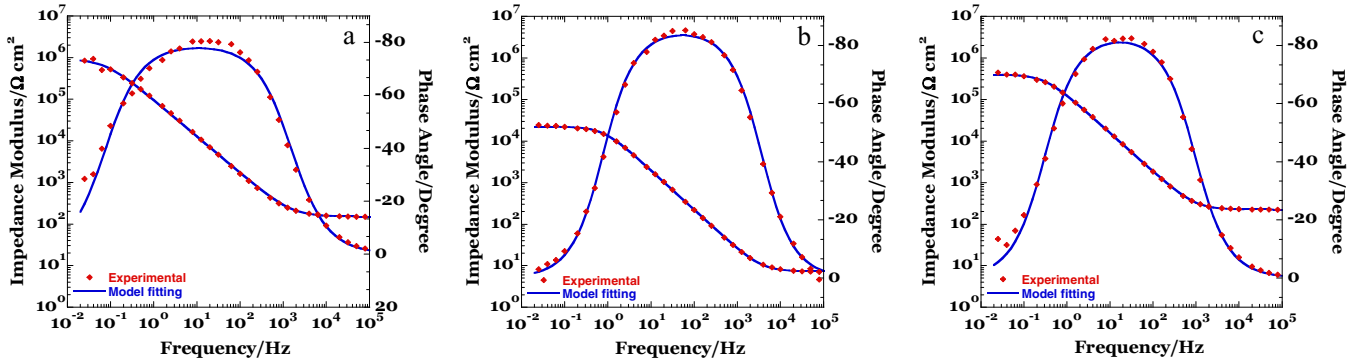

Figure 6. Typical experimental (symbols) and calculated (line) impedance spectra acquired (a) during hot water sealing, (b) during sodium chromate sealing and (c) during cerium (III) nitrate sealing.

sealing and alternative sealing methods, such as hot-water and cerium sealing.

Overall, the modifications on the porous oxide induced by sealing can be considered in two ways, namely: (i) partial dissolution of the porous oxide skeleton, and (ii) precipitation of sealing products. EIS performed during and after sealing, enables following in-situ such modifications in the various solutions. Specifically, it is evident that no significant modification of the barrier layer properties (and, by extension, of the majority of the porous skeleton) is associated with the application of any of the non-chromium containing sealing processes. This is highlighted by the fact that the capacitance of the barrier layer, and thereby its thickness, does not change substantially during sealing in chromate-free solution. Thus, the effects of such procedures are limited to the external regions of the oxide, and are likely to involve only a limited dissolution of the porous skeleton. In contrast, when sealing is performed in sodium chromate, the dissolution of the pre-existing porous skeleton is very substantial, as it is evident for the rapid increase in capacitance, associated with barrier layer thinning,

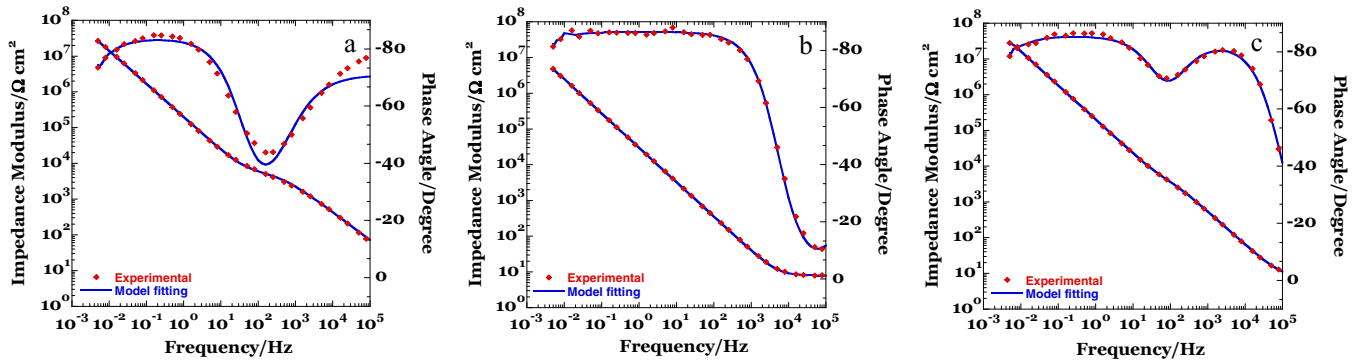

Figure 7. Typical experimental (symbols) and calculated (line) impedance spectra acquired (a) after hot water sealing, (b) after sodium chromate sealing and (c) after cerium (III) nitrate sealing.

Table II. Results of the fitting procedure, a) during sealing, b) after sealing.

a) During Sealing

Time (min)	Cold water R_{bl} $\Omega \cdot cm^2$	Cold water CPE_{bl} $s^n\ \Omega^{-1}cm^{-2}$	Cold water n	Hot water R_{bl} $\Omega \cdot cm^2$	Hot water CPE_{bl} $s^n\ \Omega^{-1}cm^{-2}$	Hot water n	Sodium Chromate R_{bl} $\Omega \cdot cm^2$	Sodium Chromate CPE_{bl} $s^n\ \Omega^{-1}cm^{-2}$	Sodium Chromate n	Cerium (III) Nitrate R_{bl} $\Omega \cdot cm^2$	Cerium (III) Nitrate CPE_{bl} $s^n\ \Omega^{-1}cm^{-2}$	Cerium (III) Nitrate n
0–6	$5.01 \cdot 10^5$	$2.10 \cdot 10^{-6}$	0.87	$4.93 \cdot 10^5$	$2.02 \cdot 10^{-6}$	0.89	$6.30 \cdot 10^3$	$2.18 \cdot 10^{-6}$	0.94	$1.53 \cdot 10^5$	$1.37 \cdot 10^{-6}$	0.93
6–12	$8.23 \cdot 10^5$	$2.17 \cdot 10^{-6}$	0.86	$7.94 \cdot 10^5$	$2.07 \cdot 10^{-6}$	0.89	$3.46 \cdot 10^3$	$9.38 \cdot 10^{-6}$	0.94	$2.68 \cdot 10^5$	$1.39 \cdot 10^{-6}$	0.93
12–18	$9.78 \cdot 10^5$	$2.23 \cdot 10^{-6}$	0.86	$8.02 \cdot 10^5$	$2.05 \cdot 10^{-6}$	0.89	$1.40 \cdot 10^4$	$1.03 \cdot 10^{-5}$	0.95	$3.22 \cdot 10^5$	$1.41 \cdot 10^{-6}$	0.93
18–24	$1.00 \cdot 10^6$	$2.22 \cdot 10^{-6}$	0.86	$9.02 \cdot 10^5$	$2.07 \cdot 10^{-6}$	0.88	$1.79 \cdot 10^4$	$1.00 \cdot 10^{-5}$	0.95	$3.54 \cdot 10^5$	$1.37 \cdot 10^{-6}$	0.93
24–30	$9.39 \cdot 10^5$	$2.18 \cdot 10^{-6}$	0.86	$9.36 \cdot 10^5$	$2.05 \cdot 10^{-6}$	0.88	$2.24 \cdot 10^4$	$9.87 \cdot 10^{-6}$	0.95	$4.03 \cdot 10^5$	$1.35 \cdot 10^{-6}$	0.93

b) After sealing

	R_{bl} $\Omega \cdot cm^2$	CPE_{bl} $s^n\ \Omega^{-1}cm^{-2}$	n	R_{seal} $\Omega \cdot cm^2$	CPE_{seal} $s^n\ \Omega^{-1}cm^{-2}$	n
Cold water	$6.79 \cdot 10^6$	$2.30 \cdot 10^{-6}$	0.94	$7.07 \cdot 10^5$	$2.30 \cdot 10^{-6}$	0.94
Hot water	$1.50 \cdot 10^8$	$9.10 \cdot 10^{-7}$	0.93	$5.12 \cdot 10^3$	$4.44 \cdot 10^{-7}$	0.78
Sodium Chromate	$7.50 \cdot 10^7$	$5.78 \cdot 10^{-6}$	0.96	7.73	$3.08 \cdot 10^{-8}$	1.00
Cerium(III) Nitrate	$2.40 \cdot 10^8$	$8.57 \cdot 10^{-7}$	0.95	$1.96 \cdot 10^3$	$1.36 \cdot 10^{-6}$	0.91

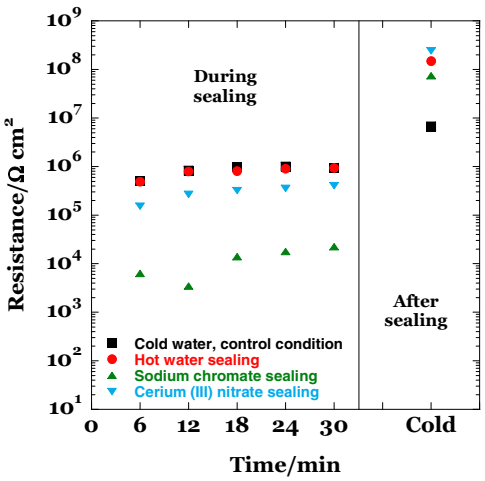

Figure 8. Time Evolution of the barrier layer resistance measured during and after sealing processes.

and corresponding decrease in resistance during the first minutes of sealing. Thus, the original porous skeleton is substantially attacked during chromium sealing, and the final properties of the sealed film are mainly determined by the properties of the re-precipitated layer. This is supported by the scanning electron microscopy observations, where the amount of precipitated material is clearly more substantial in the case of chromate sealing, and the final surface has little resemblance with the original porous film.

It is also interesting to notice that all the sealing treatments applied provide values of low-frequency impedance after sealing that are all slightly higher than those measured for sodium chromate sealing. This suggests that the barrier properties offered by the chromium sealing are in fact inferior to those provided by hot-water sealing and cerium sealing, and that the good corrosion protection offered is mainly due to the active inhibition properties of residual hexavalent chromium ions. Based on this argument, it is evident that cerium-based sealing produces a final film with barrier properties that are comparable to those offered by hot water sealing, but it has the added benefit of providing a reservoir of active species in the form of cerium ions.

Considering the experimental evidences from the perspective of the precipitation products, it is evident that cerium sealing could be an attractive candidate for hexavalent chromium sealing replacement.

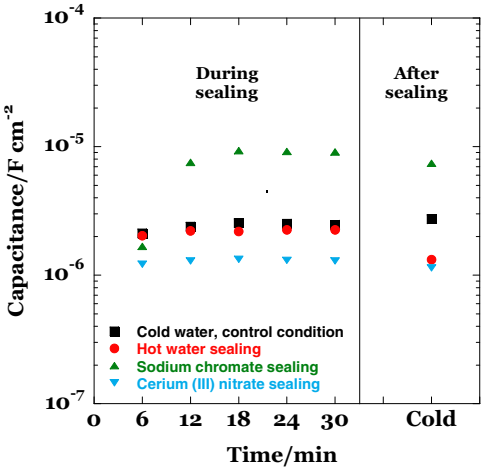

Figure 9. Time evolution of the barrier layer capacitance measured during and after sealing processes.

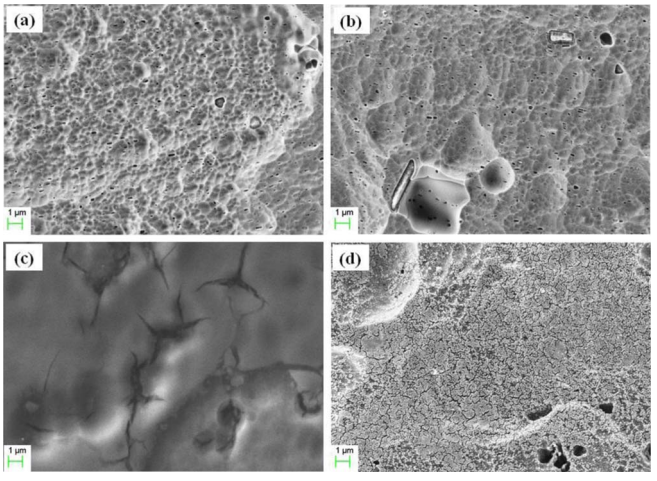

Figure 10. Scanning electron micrographs of the surface of an AA2024-T3 specimen (a) anodized, (b) hot water sealed, (c) sodium chromate sealed and (d) cerium (III) nitrate sealed.

As discussed previously, the attack of the porous oxide skeleton associated with cerium sealing is minimal, but a significant amount of precipitation products are formed, as evident both from EIS spectra (Fig. 4) and from SEM images (Fig. 10). Importantly, cerium sealing is performed at low-temperature compared to both hot water and chromium sealing, and the addition of hydrogen peroxide does not pose an environmental threat. Thus the overall environmental impact of the process is considerably reduced, both in terms of energy consumption compared to hot water sealing and in terms of use of environmentally harmful chemicals compared to chromic acid sealing.

Conclusions

In this study, electrochemical impedance spectroscopy was used to characterize in-situ the sealing behavior of an aerospace aluminum alloy anodized with the industrially accepted tartaric-sulfuric anodizing process. Electrochemical impedance spectroscopy measurements performed during sodium chromate, cerium nitrate and hot water sealing, revealed that the overall behavior is significantly different in the three solutions. In particular, during sodium chromate sealing, the porous oxide skeleton is heavily attacked by the solution, and a significant increase in capacitance is observed. This is associated with a substantial thinning of the barrier layer of the porous oxide, which is not observed during hot water and cerium nitrate sealing. On the contrary, cerium nitrate sealing does not attack the porous skeleton, but it induces the precipitation of cerium-containing compounds above the and within the pores of the anodic oxide. Overall, cerium sealing has environmental advantages compared to the other processes since it requires a much lower temperature compared to sodium chromate and hot water sealing, enable energy saving, and does not use environmentally harmful compounds such as hexavalent chromium.

Acknowledgments

The authors thank EPSRC for the support of the LATEST2 Programme grant (EP/H020047/1) and of the STEPFAR Programme grant (PON 03PE_00129_1).

References

1. E. Eichinger, J. Osborne, and T. Van Cleave, *Met. Finish.*, **95**, 36 (1997).
2. V. Moutarlier, M. P. Gigandet, L. Ricq, and J. Pagetti, *Appl. Surf. Sci.*, **183**, 1 (2001).
3. V. Moutarlier, M. P. Gigandet, J. Pagetti, and B. Normand, *Surf. Coatings Technol.*, **161**, 267 (2002).
4. European Pat. EP 1 233 084 A2 (2002).
5. M. García-Rubio, P. Ocóna, A. Climent-Font, R. W. Smith, M. Curioni, G. E. Thompson, P. Skeldon, A. Lavía, and I. García, *Corros. Sci.*, **51**, 2034 (2009).
6. V. Marzocchi, L. Iglesias-Rubianes, G. E. Thompson, and F. Bellucci, *Corros. Rev.*, **25**, 461 (2007).
7. M. Curioni, P. Skeldon, E. Koroleva, G. E. Thompson, and J. Ferguson, *J. Electrochem. Soc.*, **156**, C147 (2009).
8. G. Boisier, N. Pébère, C. Druez, M. Villatte, and S. Suel, *J. Electrochem. Soc.*, **155**, C521 (2008).
9. L. Iglesias-Rubianes, S. J. Garcia-Vergara, P. Skeldon, G. E. Thompson, and J. Ferguson, *Electrochim. Acta*, **52**, 7148 (2007).
10. W. G. Fahrenholtz, M. J. O'Keefe, H. Zhou, and J. T. Grant, *Surf. Coatings Technol.*, **155**, 208 (2002).
11. A. E. Hughes, J. D. Gorman, P. R. Miller, B. A. Sexton, P. J. K. Paterson, and R. J. Taylor, *Surf. Interface Anal.*, **36**, 290 (2004).
12. M. A. Jakab, F. Presuel-Moreno, and J. R. Scully, *J. Electrochem. Soc.*, **153**, B244 (2006).
13. A. K. Mishra and R. Balasubramaniam, *Mater. Chem. Phys.*, **103**, 385 (2007).
14. S. You, P. Jones, A. Padwal, P. Yu, and M. O'Keefe , W. Fahrenholtz and T. O'Keefe, *Mater. Lett.*, **61**, 3778 (2007).
15. I. V. Gordovskaya, T. Hashimoto, J. Walton, M. Curioni, G. E. Thompson, and P. Skeldon, *J. Electrochem. Soc.*, **161**, C601 (2014).
16. L. Hao and B. R. Cheng, *Met. Finish.*, **98**, 8 (2000).
17. V. LoF́pez, M. J. BartolomeF́, E. Escudero, E. Otero, and J. A. GonzaF́lez, *J. Electrochem. Soc.*, **153**, B75 (2006).
18. F. Mansfeld, C. Chen, C. B. Breslin, and D. Dull, *J. Electrochem. Soc.*, **145**, 2792 (1998).
19. H. Herrera-Hernandez, J. R. Vargas-Garcia, J. M. Hallen-Lopez, and F. Mansfeld, *Mater. Corros.*, **58**, 825 (2007).
20. M. R. Kalantary, D. R. Gabe, and D. H. Ross, *J. Appl. Electrochem.*, **22**, 268 (1992).
21. F. H. Scholes and C. Soste , A. E. Hughes, S. G. Hardin, and P. R. Curtis, *Appl. Surf. Sci.*, **253**, 1770 (2006).
22. M. Curioni, F. Scenini, T. Monetta, and F. Bellucci, *Electrochim. Acta*, **166**, 372 (2015).
23. M. Curioni, M. Saenz de Mier, P. Skeldon, G. E. Thompson, and J. Ferguson, *J. Electrochem. Soc.*, **155**, C387 (2008).
24. M. Saenz de Miera, M. Curioni, P. Skeldon, and G. E. Thompson, *Corros. Sci.*, **50**, 3410 (2008).
25. M. Saenz de Miera, M. Curioni, P. Skeldon, and G. E. Thompson, *Surf. Interface Anal.*, **42**, 241 (2010).
26. T. P. Hoar and G. C. Wood, *Electrochim. Acta*, **7**, 333 (1962).
27. J. Hitzig, K. Juttner, W. J. Lorenz, and W. Paatsch, *Corros. Sci.*, **24**, 945 (1984).
28. B. Hirschorn, M. E. Orazem, B. Tribollet, V. Vivier, I. Frateur, and M. Musiani, *Electrochim. Acta*, **55**, 6218 (2010).
29. M. Curioni, P. Skeldon, G. E. Thompson, and J. Ferguson, *Adv. Mater. Res.*, **3**, 48 (2008).
30. Y. Ma, X. Zhou, G. E. Thompson, M. Curioni, P. Skeldon, X. Zhang, Z. Sun, C. Luo, Z. Tang, and F. Lu, *Electrochim. Acta*, **80**, 148 (2012).